

Impact of J/ψ pair production at the LHC and predictions in nonrelativistic QCD

Li-Ping Sun^{a,*}, Hao Han^{a,†} and Kuang-Ta Chao^{a,b,c,‡}

(a) School of Physics and State Key Laboratory of Nuclear Physics and Technology, Peking University, Beijing 100871, China

(b) Collaborative Innovation Center of Quantum Matter, Beijing, China

(c) Center for High Energy physics, Peking University, Beijing 100871, China

For J/ψ pair production at hadron colliders, we present the full next-to-leading order (NLO) calculations with the color-singlet channel in nonrelativistic QCD. We find that the NLO result can reasonably well describe the LHCb measured cross section, but exhibits very different behaviors from the CMS data in the transverse momentum distribution and mass distribution of J/ψ pair. Moreover, by adding contributions of gluon fragmentation and quark fragmentation, which occur at even higher order in α_s , it is still unable to reduce the big differences. In particular, the observed flat distribution in the large invariant mass region is hard to explain. New processes or mechanisms are needed to understand the CMS data for J/ψ pair production.

PACS numbers: 12.38.Bx, 13.60.Le, 14.40.Pq

A. INTRODUCTION

Nonrelativistic QCD (NRQCD)[1] is widely used in the study of heavy quarkonium physics. In NRQCD a quarkonium production process can be factorized as short-distance parton scattering amplitudes multiplied by long-distance matrix elements (LDMEs). This factorization has been applied in single quarkonium production and tested by various experiments[2–7].

Besides the single quarkonium production, the multi-quarkonium production provides another ideal laboratory to understand the quarkonium production mechanism that NRQCD assumes. At the LHC, the LHCb Collaboration in 2011 measured the J/ψ pair production for the first time at the center-of-mass energy $\sqrt{s} = 7$ TeV with an integrated luminosity of 35.2 pb^{-1} [8]. In 2013, the CMS Collaboration further released the data of J/ψ pair production[9] with a much larger transverse momentum range, providing a good platform for testing the validity of NRQCD in quarkonium pair production.

In Refs.[10–12], the leading order (LO) calculation of J/ψ pair production in the color singlet model (CSM) is performed. The relativistic correction to the J/ψ pair production is carried out in Ref.[13], where the relativistic correction makes significant improvement for diluting the discrepancy between the shapes of color-singlet (CS) and color-octet (CO) differential cross sections at LO. Furthermore, the partial next-to-leading order (NLO*) correction for J/ψ pair production is evaluated by Lansberg and Shao [14]. They argue that the NLO* yield can approach the full NLO result at large p_T , the transverse momentum of one of the two J/ψ 's, and thus the NLO* results give a more precise theoretical prediction than the

LO results in this region. All the above works are performed in the single parton scattering (SPS) mechanism, while the contribution of double parton scattering (DPS) is assessed in Refs.[15–17], and is expected to be important. As predictions for DPS are very model-dependent [15–17], it is needed to have an accurate calculation for SPS contribution before one can extract the DPS contribution.

In order to further understand the multi-quarkonium production mechanism, it is necessary to evaluate the J/ψ pair production at NLO, which is the main work in this paper. Compared to the LO calculation, the NLO calculation is expected to not only reduce the theoretical uncertainties, but also open new kinematic enhanced topologies, which may dominate at large p_T . More precisely, we may find that at NLO the differential cross section $d\sigma/dp_T^2$ at large p_T behaves as p_T^{-6} due to double parton fragmentation contributions [18], while it only behaves as p_T^{-8} at LO. Moreover, we also include the dominant p_T^{-4} contribution via single parton fragmentation, which contributes at even higher order in α_s and also involves color-octet channels. Thus we will obtain the most precise predictions for J/ψ pair production with the color-singlet channel as well as some color-octet effects in the fragmentation contributions.

B. FORMULISM

In NRQCD, the cross section of J/ψ pair production at the LHC can be expressed as [1]

$$d\sigma_{p+p \rightarrow J/\psi+J/\psi} = \sum_{i,j,n_1,n_2} \int dx_1 dx_2 f_{i/p}(x_1) f_{j/p}(x_2) \times d\hat{\sigma}_{i,j}^{n_1,n_2} \langle \mathcal{O}_{n_1} \rangle^{J/\psi} \langle \mathcal{O}_{n_2} \rangle^{J/\psi}. \quad (1)$$

where $f_{i/p}(x_{1,2})$ are the parton distribution functions (PDFs), x_1 and x_2 represent the momentum fraction of initial state partons from the protons, $\langle \mathcal{O}_n \rangle^{J/\psi}$ are

*Electronic address: sunliping@pku.edu.cn

†Electronic address: hao.han@pku.edu.cn

‡Electronic address: ktchao@pku.edu.cn

LDMEs of J/ψ with $n = {}^{2S+1}L_J^{[c]}$ are the standard spectroscopic notation for the quantum numbers of the produced intermediate heavy quark pairs, and $d\hat{\sigma}$ are partonic short distance coefficients. For the J/ψ pair production we usually set $n_1 = n_2 = {}^3S_1^{[1]}$ in Eq. (1) but other intermediate states may also be specified.

In the LO calculation, there are two subprocesses: $g + g \rightarrow J/\psi + J/\psi$ and $q + \bar{q} \rightarrow J/\psi + J/\psi$, only the former is taken into account since the contribution of the other process is highly suppressed by the quark PDFs. While in the NLO case, besides the gluon fusion process, the quark gluon process $q + g \rightarrow 2J/\psi + q$ should also be considered. Typical Feynman diagrams at LO and NLO are shown in Fig.1 (a) – (c).

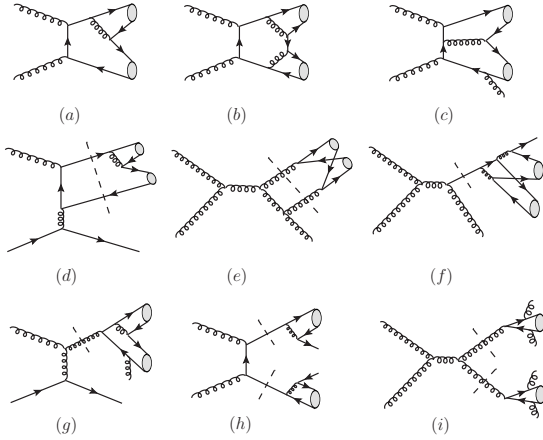


FIG. 1: Typical Feynman diagrams for J/ψ pair production in color-singlet channel, including LO, NLO, as well as single quark or gluon fragmentation diagrams beyond NLO.

The $c\bar{c}$ pair hadronization process can be computed by using the covariant projection operator method, for $J/\psi({}^3S_1)$, we employ the following commonly used projection operators for spin and color:

$$\Pi_1 = \frac{1}{\sqrt{8m_c^3}} \left(\frac{\not{P}}{2} - m_c \right) \not{\epsilon}_{J/\psi} \left(\frac{\not{P}}{2} + m_c \right). \quad (2)$$

and

$$\mathcal{C}_1 = \frac{1}{\sqrt{N_c}}. \quad (3)$$

where $\epsilon_{J/\psi}^\mu$ is the J/ψ polarization vector with $P \cdot \epsilon = 0$, P is the momentum of J/ψ .

The NLO contributions can be divided into two parts: the virtual correction and the real correction. The virtual correction which arises from loop diagrams includes gluon fusion process only, the same as the LO case, while for the real correction, besides the gluon fusion process, the process $q + g \rightarrow 2J/\psi + q$ should also be taken into account.

In the virtual correction, the ultraviolet(UV) and infrared(IR) divergences usually exist. We use the dimensional regularization scheme to regularize the UV and

IR divergences. The Coulomb divergence caused by the virtual gluon line connecting the quark pair in a J/ψ , is regularized by the relative velocity v . The UV divergences can be renormalized by counter terms. The renormalization constants include Z_2 , Z_3 , Z_m , and Z_g , corresponding to quark field, gluon field, quark mass, and strong coupling constant α_s , respectively. Here, in our calculation the Z_g is defined in the modified-minimal-subtraction ($\overline{\text{MS}}$) scheme, while for the other three the on-shell (OS) scheme is adopted, which reads

$$\begin{aligned} \delta Z_m^{OS} &= -3C_F \frac{\alpha_s}{4\pi} \left[\frac{1}{\epsilon_{UV}} - \gamma_E + \ln \frac{4\pi\mu_r^2}{m_c^2} + \frac{4}{3} \right], \\ \delta Z_2^{OS} &= -C_F \frac{\alpha_s}{4\pi} \left[\frac{1}{\epsilon_{UV}} + \frac{2}{\epsilon_{IR}} - 3\gamma_E + 3 \ln \frac{4\pi\mu_r^2}{m_c^2} + 4 \right], \\ \delta Z_{2l}^{OS} &= -C_F \frac{\alpha_s}{4\pi} \left[\frac{1}{\epsilon_{UV}} - \frac{1}{\epsilon_{IR}} \right], \\ \delta Z_3^{OS} &= \frac{\alpha_s}{4\pi} \left[(\beta'_0 - 2C_A) \left(\frac{1}{\epsilon_{UV}} - \frac{1}{\epsilon_{IR}} \right) \right. \\ &\quad \left. - \frac{4}{3} T_F (n_f - n_{lf}) \left(\frac{1}{\epsilon_{UV}} - \gamma_E + \ln \frac{4\pi\mu_r^2}{m_c^2} \right) \right], \\ \delta Z_g^{\overline{\text{MS}}} &= -\frac{\beta_0}{2} \frac{\alpha_s}{4\pi} \left[\frac{1}{\epsilon_{UV}} - \gamma_E + \ln(4\pi) \right]. \end{aligned} \quad (4)$$

where $\beta_0 = \frac{11}{3}C_A - \frac{4}{3}T_F n_f$ is the one-loop coefficient of the QCD beta function; $n_f = 4$ is the number of active quarks in our calculation; $\beta'_0 = \frac{11}{3}C_A - \frac{4}{3}T_F n_{lf}$ with $n_{lf} = 3$ the number of light quarks. $C_A = 3$ and $T_F = 1/2$ attributed to the SU(3) group; μ_r is the renormalization scale.

As mentioned above, there are two processes involved in the real corrections: $g + g \rightarrow J/\psi + J/\psi + g$ and $q + g \rightarrow J/\psi + J/\psi + q$. It is known that IR divergence exists in these processes because of the phase space integration, which can be canceled by the IR singularities left in the virtual correction. According to the different regions of the phase space, the IR divergence can be categorized as soft or collinear. In this paper, we use the two-cutoff phase space slicing method[19] to isolate the two types of IR singularities, then the cross section of real correction can be expressed as:

$$\sigma_{Real} = \sigma_{Real}^{Soft} + \sigma_{Real}^{HC} + \sigma_{Real}^{\overline{HC}}. \quad (5)$$

where HC and \overline{HC} represent hard collinear and hard non-collinear contributions, respectively.

The soft singularities only originate from real gluon emission, that is, the $g(p_1) + g(p_2) \rightarrow J/\psi(p_3) + J/\psi(p_4) + g(p_5)$ process. p_5 is the momentum of the emitted gluon, and in the $p_1 + p_2$ rest frame, $p_1 + p_2 = \sqrt{s_{12}}(1, 0, 0, 0)$. Applying the two cutoff technique, the soft region is defined in the $p_1 + p_2$ rest frame by $0 \leq E_5 \leq \delta_s \sqrt{s_{12}}/2$, where δ_s is a small cut.

In the soft region, the three-body phase space can be

simplified as:

$$\begin{aligned} d\text{PS}_3|_{\text{soft}} &= d\text{PS}_2 \frac{d^{d-1}p_5}{2p_5^0(2\pi)^{d-1}}|_{\text{soft}} \\ &= d\text{PS}_2 \left[\left(\frac{4\pi}{s_{12}} \right)^\epsilon \frac{\Gamma(1-\epsilon)}{\Gamma(1-2\epsilon)} \frac{1}{2(2\pi)^2} \right] dS. \end{aligned} \quad (6)$$

with

$$\begin{aligned} dS &= \frac{1}{\pi} \left(\frac{4}{s_{12}} \right)^{-\epsilon} \int_0^{\delta_s \sqrt{s_{12}}/2} dE_5 E_5^{1-2\epsilon} \\ &\times \sin^{1-2\epsilon}\theta_1 d\theta_1 \sin^{-2\epsilon}\theta_2 d\theta_2. \end{aligned} \quad (7)$$

Meanwhile, the relative matrix elements in the soft region can be factorized as

$$M_3^a|_{\text{soft}} \simeq g\mu_r^\epsilon \varepsilon^\mu(p_5) \mathbf{J}_\mu^a(p_5) \mathbf{M}_2, \quad (8)$$

where a is the color index the emitted gluon carries, and $\varepsilon^\mu(p_5)$ is the gluon's polarization vector. \mathbf{M}_2 is the color connected LO Born matrix element, $\mathbf{J}_\mu^a(p_5)$ is the non-abelian eikonal current, which contains the color structure of the emitted gluon and the soft divergence information. The concrete form of $\mathbf{J}_\mu^a(p_5)$ is given by:

$$\mathbf{J}_\mu^a(p_5) = \sum_f \mathbf{T}_f^a \frac{p_f}{p_f \cdot p_5}, \quad (9)$$

where the sum goes over each external line that can emit a soft gluon, the color structure associated with each soft gluon emission from parton f is denoted by \mathbf{T}_f . Then the squared matrix element reads:

$$|M_3|^2|_{\text{soft}} \simeq -g^2 \mu_r^{2\epsilon} \sum_{f,f'} \frac{p_f \cdot p_{f'}}{p_f \cdot p_5 p_{f'} \cdot p_5} M_{ff'}^0, \quad (10)$$

with

$$\begin{aligned} M_{ff'}^0 &= (\mathbf{T}_f^a \mathbf{M}_2) (\mathbf{T}_{f'}^a \mathbf{M}_2) \\ &= \left[M_{c_1 \dots b_f \dots b_{f'} \dots c_4} \right]^* T_{b_f d_f}^a T_{b_{f'} d_{f'}}^a M_{c_1 \dots d_f \dots d_{f'} \dots c_4}. \end{aligned} \quad (11)$$

Combining the phase space and squared matrix element given above, one can finally get the cross section of real correction in the soft region:

$$\begin{aligned} d\sigma_{\text{Real}}^{\text{Soft}} &= \left[\frac{\alpha_s}{2\pi} \frac{\Gamma(1-\epsilon)}{\Gamma(1-2\epsilon)} \left(\frac{4\pi\mu_r^2}{s_{12}} \right)^\epsilon \right] \sum_{f,f'} d\sigma_{ff'}^{\text{Born}} \\ &\times \int \frac{-p_f \cdot p_{f'}}{p_f \cdot p_5 p_{f'} \cdot p_5} dS, \end{aligned} \quad (12)$$

with

$$d\sigma_{ff'}^{\text{Born}} \propto \overline{\sum} M_{ff'}^0 d\text{PS}_2. \quad (13)$$

We can see in Eq. (12) that in the soft region, the divergence is singled out. All the concrete expressions of

the integration $\int \frac{-p_f \cdot p_{f'}}{p_f \cdot p_5 p_{f'} \cdot p_5} dS$ are listed in the Appendix of Ref.[19].

The hard collinear divergence only occurs at massless case, so it is also called ‘‘mass singularity’’. According to the two cutoff method, a small cut δ_c is brought in, and the hard collinear region of the phase space is that where any invariants (s_{ij} or t_{ij}) gets smaller than $\delta_c s_{12}$. The hard-collinear divergence can be divided into initial state collinear and final state collinear, depending on the singularities from initial or final state. For our process, there is only initial state collinear because the J/ψ pair in the final state are massive. The processes include: $g(p_1) + g(p_2) \rightarrow J/\psi(p_3) + J/\psi(p_4) + g(p_5)$ and $g(p_1) + q(p_2) \rightarrow J/\psi(p_3) + J/\psi(p_4) + q(p_5)$. Hereafter, we only consider the case that the emitting and splitting occur at parton $g(p_2)$ and $q(p_2)$, that is, $0 \leq t_{25} = (p_2 - p_5)^2 \leq \delta_c s_{12}$, the other cases are tackled the same way.

In the hard-collinear region, the three-body phase space can be written as:

$$\begin{aligned} d\text{PS}_3|_{HC} &= \left[\frac{d^{d-1}p_3}{2p_3^0(2\pi)^{d-1}} \frac{d^{d-1}p_4}{2p_4^0(2\pi)^{d-1}} \right. \\ &\times (2\pi)^d d^d(p_1 + zp_2 - p_3 - p_4) \left. \right] \frac{d^{d-1}p_5}{2p_5^0(2\pi)^{d-1}}. \end{aligned} \quad (14)$$

where z is the momentum fraction for the splitting $2 \rightarrow 2' + 5$, by applying the collinear approximation, the three-body matrix elements can be expressed as follows:

$$\begin{aligned} &\overline{\sum} |M_3(1+2 \rightarrow 3+4+5)|^2 \\ &\simeq \overline{\sum} |M_2(1+2' \rightarrow 3+4)|^2 P_{2'2}(z, \epsilon) g^2 \mu_r^{2\epsilon} \frac{-2}{zt_{25}}. \end{aligned} \quad (15)$$

Combining the phase space and the matrix elements, we can obtain the cross section in the hard collinear region:

$$\begin{aligned} d\sigma_{\text{Real}}^{HC}(p+p \rightarrow 2J/\psi + X) &= \sum_{i=g,q} f_{g/p}(x_1) f_{i/p}(x_2/z) \left[\frac{\alpha_s}{2\pi} \frac{\Gamma(1-\epsilon)}{\Gamma(1-2\epsilon)} \left(\frac{4\pi\mu_r^2}{s_{12}} \right)^\epsilon \right] \\ &\times d\hat{\sigma}_0^{\text{Born}} \left(-\frac{1}{\epsilon} \right) \delta_c^{-\epsilon} P_{gi}(z, \epsilon) \frac{dz}{z} \left[\frac{(1-z)}{z} \right]^{-\epsilon} dx_1 dx_2. \end{aligned} \quad (16)$$

The collinear singularity emerging in Eq. (16) should be factorized into the parton distribution functions. To do this, a scale dependent parton distribution function is introduced using the $\overline{\text{MS}}$ convention:

$$\begin{aligned} f_{b/B}(x, \mu_f) &= f_{b/B}(x) - \frac{1}{\epsilon} \left[\frac{\alpha_s}{2\pi} \frac{\Gamma(1-\epsilon)}{\Gamma(1-2\epsilon)} \left(\frac{4\pi\mu_r^2}{\mu_f^2} \right)^\epsilon \right] \\ &\times \int_z^1 \frac{dz}{z} P_{bb'}(z) f_{b'/B}(x/z). \end{aligned} \quad (17)$$

After renormalization of the parton distribution function, we can eventually obtain the cross section for the initial state collinear contribution:

$$\begin{aligned}
& d\sigma_{Real}^{HC}(p+p \rightarrow 2J/\psi + X) \\
&= d\hat{\sigma}_0^{Born} \left[\frac{\alpha_s}{2\pi} \frac{\Gamma(1-\epsilon)}{\Gamma(1-2\epsilon)} \left(\frac{4\pi\mu_f^2}{s_{12}} \right)^\epsilon \right] \\
&\times \left\{ f_{g/p}(z_1, \mu_f) \tilde{f}_{g/p}(z_2, \mu_f) + \left[\frac{A_1^{SC}(g \rightarrow g+g)}{\epsilon} \right. \right. \\
&\left. \left. + A_0^{SC}(g \rightarrow g+g) \right] f_{g/p}(z_1, \mu_f) f_{g/p}(z_2, \mu_f) \right\} dz_1 dz_2.
\end{aligned} \tag{18}$$

Note that in this expression, the collinear singularity is absorbed into the redefinition of the parton distribution function. The left soft collinear factors A_i^{SC} result from the difference of the upper bound of the z integration in Eq.(16) and Eq.(17). These factors are given by:

$$\begin{aligned}
A_1^{SC}(g \rightarrow g+g) &= 2N \ln \delta_s + (11N - 2n_f)/6, \\
A_0^{SC}(g \rightarrow g+g) &= [2N \ln \delta_s + (11N - 2n_f)/6] \ln \left(\frac{s_{12}}{\mu_f^2} \right).
\end{aligned} \tag{19}$$

There is no $A_i^{SC}(q \rightarrow q+g)$ term existing because the $q \rightarrow q+g$ splitting process demonstrates no soft singularities. The \tilde{f} functions read:

$$\tilde{f}_{g/p}(z, \mu_f) = \sum_i \int_z^{1-\delta_s \delta_{gi}} \frac{dy}{y} f_{i/p}\left(\frac{z}{y}, \mu_f\right) \tilde{P}_{gi}(y), \tag{20}$$

with

$$\tilde{P}_{ij}(y) = P_{ij}(y) \ln \left(\delta_c \frac{1-y}{y} \frac{s_{12}}{\mu_f^2} \right) - P'_{ij}(y). \tag{21}$$

where the index i in the sum represents a gluon or a quark, and the d-dimension unregulated splitting functions $P_{ij}(y)$ and $P'_{ij}(y)$ are given by:

$$\begin{aligned}
P_{qq}(y) &= C_F \frac{1+y^2}{1-y}, \\
P'_{qq}(y) &= -C_F(1-y), \\
P_{gq}(y) &= C_F \frac{1+(1-y)^2}{y}, \\
P'_{gq}(y) &= -C_F y, \\
P_{gg}(y) &= 2N \left[\frac{y}{1-y} + \frac{1-y}{y} + y(1-y) \right], \\
P'_{gg}(y) &= 0, \\
P_{qg}(y) &= \frac{1}{2} [y^2 + (1-y)^2], \\
P'_{qg}(y) &= -y(1-y).
\end{aligned} \tag{22}$$

Now, the cross sections for the J/ψ pair production at NLO can be expressed as:

$$\sigma_{NLO} = \sigma_{Born} + \sigma_{Virtual} + \sigma_{Real}. \tag{23}$$

The soft divergences and collinear divergences from real corrections will cancel divergences from virtual corrections, and thus the final NLO contributions are IR safe.

Because there are two J/ψ states in the final state, the LO contributions behave as p_T^{-8} when p_T is large. However, at NLO level, there are double quark and double gluon fragmentation contributions [Fig. 1 (d) and (e)], which give p_T^{-6} behavior [18]. We thus expect that the NLO contribution will dominate at large p_T , especially for the CMS data, where a relatively large lower p_T cut-off is taken [9]. Since in the double parton fragmentation diagrams the two J/ψ 's come from the same fragmenting partons, the invariant mass of the pair (denoted as $M_{J/\psi J/\psi}$) should be small. This implies that the NLO correction will be significant only in the small $M_{J/\psi J/\psi}$ region, and it will be mild when $M_{J/\psi J/\psi}$ is large. All these expectations will be confirmed by our numerical results shown below.

When p_T is large enough, the single parton fragmentation contributions, which behave as p_T^{-4} , will eventually dominate, although they are suppressed by powers of α_s . For double J/ψ production, the quark and gluon fragmentation processes can be expressed as

$$\begin{aligned}
d\sigma_{A+B \rightarrow 2J/\psi + X} &= \sum_{i,j,n_1,n_2} d\hat{\sigma}_{A+B \rightarrow i+j+X} \\
&\otimes D_{i \rightarrow Q\bar{Q}(n_1)} \otimes D_{j \rightarrow Q\bar{Q}(n_2)} \langle \mathcal{O}_{n_1} \rangle \langle \mathcal{O}_{n_2} \rangle,
\end{aligned} \tag{24}$$

where $D_{i,j \rightarrow Q\bar{Q}(n)}$ are the single-parton fragmentation functions (FFs) for a NRQCD state n . Typical Feynman diagrams for these kinds of fragmentation contributions are shown in Fig.1 (h) and (i). These FFs are factorization scale dependent, and satisfy the DGLAP evolution equation [21–25]

$$\frac{d}{d \log \mu_f^2} \begin{pmatrix} D_c \\ D_g \end{pmatrix} = \frac{\alpha_s(\mu_f)}{2\pi} \begin{pmatrix} P_{cc} & P_{gc} \\ P_{cg} & P_{gg} \end{pmatrix} \otimes \begin{pmatrix} D_c \\ D_g \end{pmatrix}, \tag{25}$$

where D_g and D_c denote the FFs from gluon and charm quark, respectively, and P_{ij} 's are the splitting functions. Based on this evolution equation, we only need inputs of FFs at an initial scale, which can be found in Ref.[20]. Note that fragmentation functions in color-octet channels will also be considered in Eq. (24).

In addition, there are also p_T^{-4} contributions coming from Feynman diagrams like Fig.1 (f) and (g), where one parton fragments to a J/ψ pair. We will argue later that these contributions should not be important.

C. Numerical Inputs

Because of the complexity of the J/ψ pair production, in our calculation, the package FEYNARTS [26] is used to generate the Feynman diagrams and amplitudes. The phase space integration is evaluated by employing the package Vegas.

In numerical calculation, the CTEQ6L1 and CTEQ6M parton distribution functions [27, 28] are used. The renormalization scale μ_r and factorization scale μ_f are chosen as $\mu_r = \mu_f = m_T$, with $m_T = \sqrt{p_T^2 + 16m_c^2}$ and charm quark mass $m_c = M_{J/\psi}/2 = 1.55$ GeV. In the two cutoff method, there are soft and collinear cutoffs, δ_s and δ_c , which we set to be $\delta_s = 10^{-2}$ and $\delta_c = 10^{-4}$. Theoretical uncertainties are estimated by varying $\mu_r = \mu_f$ from $m_T/2$ to $2m_T$.

The CS LDME $\langle \mathcal{O}(^3S_1^{[1]}) \rangle^{J/\psi} = 1.16 \text{ GeV}^3$ is estimated by using the B-T potential model [29]. While CO LDMEs for $^1S_0^{[8]}$, $^3S_1^{[8]}$ and $^3P_0^{[8]}$ channels, which are needed in fragmentation processes, are taken from three different extractions [30–32]. Meanwhile, the $^1S_0^{[8]}$ -dominant CO matrix elements extracted from [33] are also taken into account.

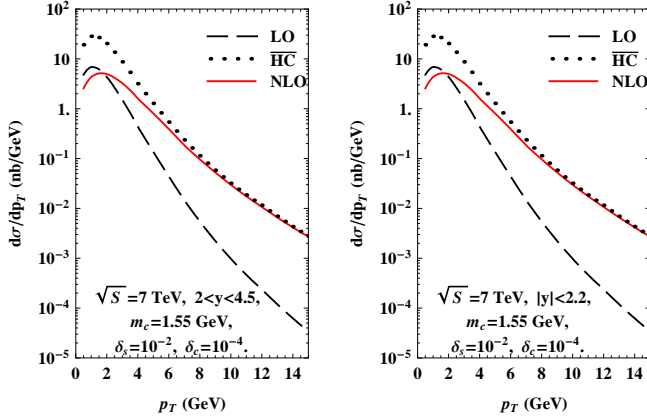


FIG. 2: (color online). Comparison between LO, \overline{HC} , and full NLO results of the cross section p_T distribution in J/ψ pair production.

D. RESULTS

To see the importance of NLO calculation, we show the cross section p_T distribution of one of the two J/ψ 's in Fig. 2 for both forward region and central region in rapidity. In the low p_T region, although NLO results are close to LO results, their behaviors are different. Especially, the NLO result peaks at a larger p_T than that of LO result. When $p_T \gtrsim 5 \text{ GeV}$, NLO results become much larger than the LO one. As emphasized above, the large NLO corrections are due to the p_T^{-6} contributions from double parton fragmentation. To demonstrate this point, we show also the hard noncollinear contributions of real correction $\sigma_{\overline{HC}_{Real}}^{J/\psi}$, which contain all the p_T^{-6} contributions,

in Fig. 2. As expected, the hard noncollinear contributions approach the full NLO result as p_T becomes larger. As for the NLO* result in Ref. [14], which introduces cutoffs to regularize soft and collinear divergences in the real corrections, it should be similar to our hard noncollinear contributions. So the NLO* result can give a good approximation to the full NLO result for double J/ψ production in the high p_T region. But the problem of infrared divergence and cutoff dependence at NLO* is removed in our full NLO calculation.

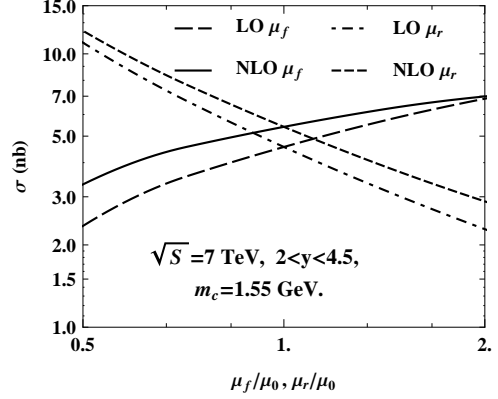


FIG. 3: (color online). Scales dependence of total cross sections for LO and NLO at LHCb, where $\mu_0 = m_T$.

At the LHCb window with $\sqrt{S} = 7 \text{ TeV}$, $2 < y(J/\psi) < 4.5$, and $0 < p_T < 10 \text{ GeV}$, the measured value is $\sigma_{J/\psi J/\psi} = 5.1 \pm 1.0 \pm 1.1 \text{ nb}$ [8]. Our calculated cross sections at LO and NLO are shown in Fig. 3, as functions of μ_r and μ_f . It can be seen that both μ_r dependence and μ_f dependence are reduced at NLO level. To avoid large logarithms of $\ln(\mu_r/\mu_f)$, as in the literature one usually estimates theoretical uncertainties by keeping $\mu_r = \mu_f$ and varying them from $m_T/2$ to $2m_T$. In this way, our predictions are $\sigma_{\text{LO}} = 4.56 \pm 1.13 \text{ nb}$ and $\sigma_{\text{NLO}} = 5.41^{+2.73}_{-1.14} \text{ nb}$, which are roughly compatible with the LHCb measured cross section.

The invariant mass distribution at LHCb is shown in Fig. 4. We see that both the LO and NLO results are inconsistent with the LHCb data, indicating that the behaviors at both LO and NLO are very different from the LHCb data, which peaks at small invariant mass and decreases more slowly than the theoretical predictions at large invariant mass. We therefore draw the conclusion that the full NLO calculation in the CS model can not describe the LHCb data.

In the CMS conditions [9]:

$$\begin{aligned} &|y(J/\psi)| < 1.2 \text{ for } p_T > 6.5 \text{ GeV, or} \\ &1.2 < |y(J/\psi)| < 1.43 \text{ for } p_T > 6.5 \rightarrow 4.5 \text{ GeV, or} \\ &1.43 < |y(J/\psi)| < 2.2 \text{ for } p_T > 4.5 \text{ GeV,} \end{aligned}$$

the total cross section is measured to be

$$\sigma_{Exp.} = 1.49 \pm 0.07 \pm 0.14 \text{ nb}, \quad (26)$$

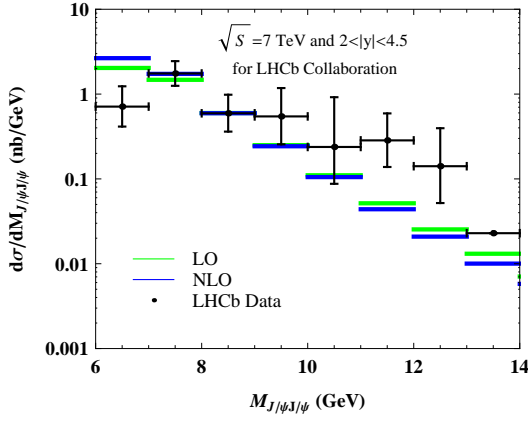


FIG. 4: (color online). Differential cross sections in bins of the J/ψ pair invariant mass at LHCb. The data are taken from Ref. [8]. The green and blue lines denote the LO and NLO theoretical results respectively.

while our LO and NLO calculations for the total cross section give

$$\sigma_{\text{LO}} = 0.08 \pm 0.02 \text{ nb}, \quad \sigma_{\text{NLO}} = 0.93 \pm 0.25 \text{ nb}. \quad (27)$$

As expected, we see the NLO calculation gives the dominant contribution. In Eq.(27) the contribution of feed-down process $p + p \rightarrow J/\psi + \psi(2S) + X \rightarrow 2J/\psi + X$ is also included, which is estimated to be 30% of the direct production[12]. Comparing Eq.(26) with Eq.(27), we see the theoretical result is inconsistent with the experimental data.

We then compare our prediction for the transverse momentum $p_{TJ/\psi J/\psi}$ distribution of J/ψ pair with data. The result is shown in Fig. 5. At LO, $p_{TJ/\psi J/\psi}$ is always zero, because it is a two-body final state process. At NLO, unfortunately, as indicated in Fig. 5, the theoretical result is still very different from the CMS data. The data obviously overshoots our NLO prediction at large $p_{TJ/\psi J/\psi}$.

As mentioned before, the single parton fragmentation processes behave as p_T^{-4} , which may give larger contributions at very large $p_{TJ/\psi J/\psi}$. We thus evaluate the single parton fragmentation contribution according to Eq. (24), and the results are shown in Fig. 5. It can be seen that, however, the fragmentation contribution is negligible even when $p_{TJ/\psi J/\psi}$ is as large as 30 GeV, no matter which set of CO LDMEs is chosen. This phenomenon seems to be surprising, but actually is not new. Similar behavior was found in Refs. [33, 34] for the single J/ψ inclusive production, where the p_T^{-6} contribution still dominates over the p_T^{-4} contribution even when p_T is 15 times larger than the mass of J/ψ . Here, the smallness of the single parton fragmentation contribution for double J/ψ production is again due to the current experimental $p_{TJ/\psi J/\psi}$ being not large enough to make fragmentation dominant. Similarly, we also do not expect the same-side-fragmentation contribution, e.g. in Fig. 1

(f) and (g), to be able to solve the surplus problem for the CMS large $p_{TJ/\psi J/\psi}$ data.

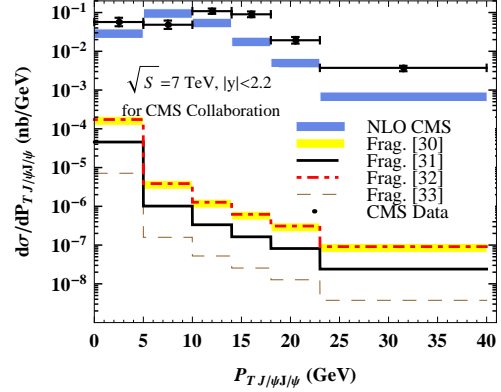


FIG. 5: (color online). Differential cross sections in bins of the transverse momentum of J/ψ pair at CMS. The data are taken from Ref. [9]. The blue band denotes the NLO results, where the uncertainties are due to scale choices as mentioned in the text, and the yellow band, solid, dash dotted lines represent the fragmentation contributions including all relevant channels by three sets of different CO matrix elements. The dashed line represents the fragmentation contribution by taking the $^1S_0^{[8]}$ -dominant CO matrix elements.

The invariant mass distribution at CMS is shown in Fig. 6. We see that the NLO result can well describe the first two bins, but it decreases too fast beginning from the third bin. This indicates that the behavior at NLO is very different from the CMS data: the latter is almost flat at large invariant mass, and larger than the NLO result by several orders of magnitude. In fact, when $22 \text{ GeV} < M_{J/\psi J/\psi} < 35 \text{ GeV}$, the NLO prediction is less than CMS data by almost two orders of magnitude, and when $35 \text{ GeV} < M_{J/\psi J/\psi} < 80 \text{ GeV}$, the discrepancy raises to almost four orders of magnitude.

Intuitively, by examining the discrepancy in the J/ψ pair mass distribution, a large angle J/ψ pair production process is apparently needed. The quark and gluon fragmentation processes shown in Fig.1(h) and Fig.1(i) are typically among the large angle processes. We then evaluate these fragmentation contributions, including all relevant color-singlet and color-octet channels (Fig.1(f) and Fig.1(g) are neglected because they are not large angle scattering processes and contribute little to the large invariant mass distribution). The total contribution of all concerned fragmentation channels is shown in Fig. 6. Unfortunately, the fragmentation contributions are found to be negligible to the J/ψ pair production, thus the discrepancy between NLO result and CMS data can not be resolved by these processes.

We also consider other possible sources for the discrepancy, e.g., the Z^0 boson decays to a J/ψ pair: $Z^0 \rightarrow 2J/\psi + X$. Under the CMS condition, the total cross section of this process is $\sigma = 2.5 \times 10^{-4} \text{ nb}$. Its contribution to each bin of the J/ψ pair transverse

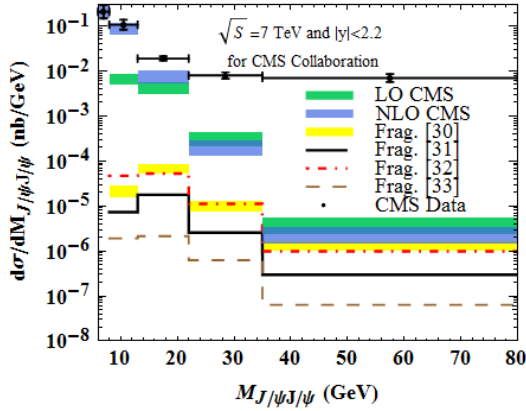


FIG. 6: (color online). Differential cross sections in bins of the J/ψ pair invariant mass at CMS. The data are taken from Ref. [9]. The green and blue bands denote the LO and NLO theoretical results respectively, where the uncertainties are due to scale choices as mentioned in the text. The yellow band, solid, dash dotted lines represent the sum of the quark and gluon fragmentation from all relevant channels by three group of different color-octet (CO) matrix elements. The dashed line represents the fragmentation contribution by taking the $^1S_0^{[8]}$ -dominant CO matrix elements.

momentum distribution or invariant mass distribution is negligibly small. So the big gap between NLO predictions and CMS data still remains.

The J/ψ pair rapidity difference $|\Delta y|$ distribution at CMS is shown in Fig. 7. We see that the NLO result can well describe the first four bins, but it decreases too fast beginning from the fifth bin. This is the same as the mass distribution, because the large mass is equivalent to the large $|\Delta y|$, and the color-singlet contributes little to a large angle scattering process. Therefore, the fragmentation contributions are also negligible in resolving the discrepancy between NLO result and CMS data, so we do not label them in this figure.

E. SUMMARY

In the framework of NRQCD factorization, we evaluate the full NLO J/ψ pair production via the color-singlet channel. We demonstrate that NLO corrections are essential for J/ψ pair production both in low p_T and high p_T regions, as compared to the LO results. Our NLO calculation can give a reasonably good description for the total cross section observed by LHCb. However, the NLO predictions of $p_{TJ/\psi J/\psi}$ distribution, invariant mass distribution of J/ψ pair, and rapidity difference distribution of J/ψ pair are very different from the CMS data. For the J/ψ pair invariant mass distribution, the observed flatness and orders of magnitude differences from theoretical predictions in the large invariant mass region ($22 \text{ GeV} < M_{J/\psi J/\psi} < 80 \text{ GeV}$) are hard to explain in NLO NRQCD with color-singlet contributions, and the

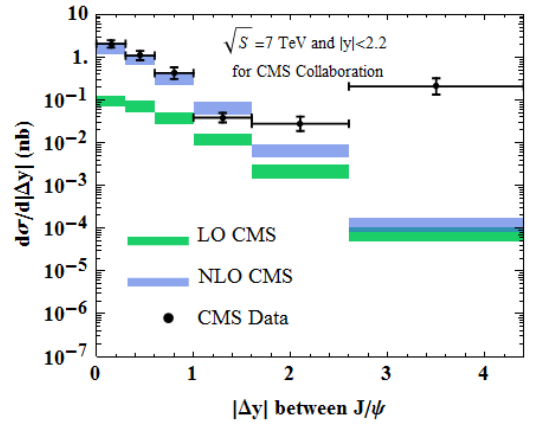


FIG. 7: (color online). Differential cross sections in bins of the J/ψ pair $|\Delta y|$ at CMS. The data are taken from Ref. [9]. The green and blue bands denote the LO and NLO theoretical results respectively, where the uncertainties are due to scale choices as mentioned in the text.

situation for rapidity difference distribution is similar to the mass distribution. This strongly indicates that the CS model cannot solve the problems not only for the well known single J/ψ inclusive production but also for the double J/ψ production at hadron colliders. We further take into account the contributions from quark fragmentation and gluon fragmentation with both CS and CO channels beyond NLO in α_s , but find they cannot provide a sizable contribution to the large angle production of the J/ψ pair. Our calculation implies that at low p_T the color-singlet contribution may be dominant but the color-octet contribution may be important at large p_T , as shown in Ref.[35] with LO color-octet calculations. Apparently, new processes or mechanisms are needed to simultaneously enlarge the total cross section, improve the $p_{TJ/\psi J/\psi}$ distribution, and increase the large invariant mass distribution and large rapidity difference distribution of J/ψ pair, if the CMS data are confirmed.

F. ACKNOWLEDGMENTS

We thank Y. Q. Ma, C. Meng, H. S. Shao, and Y. J. Zhang for valuable discussions and suggestions, and J.P. Lansberg for useful communications. This work was supported in part by the National Natural Science Foundation of China (No 11475005, No 11075002), and the National Key Basic Research Program of China (No. 2015CB856700).

-
- [1] G. T. Bodwin, E. Braaten, and G. P. Lepage, Phys. Rev. D **51**, 1125(1995).
 - [2] M. Butenschoen, and B. A. Kniehl, AIP Conf. Proc. **1343**, 409 (2011); M. Butenschoen, and B. A. Kniehl, Phys. Rev. Lett. **107**, 232001 (2011); M. Butenschoen, and B. A. Kniehl, Phys. Rev. Lett. **108**, 172002 (2012).
 - [3] M. Butenschoen, and B. A. Kniehl, Mod. Phys. Lett. A **28**, 1350027 (2013); M. Butenschoen, Z. G. He and B. A. Kniehl, Phys. Rev. D **88**, 011501 (2013); B. A. Kniehl, and M. Butenschoen, PoS ICHEP2012, **278** (2013).
 - [4] Y. Fan, Y. Q. Ma and K. T. Chao, Phys. Rev. D **79**, 114009 (2009); Y. J. Zhang, Y. Q. Ma, K. Wang and K. T. Chao, Phys. Rev. D **81**, 034015 (2010); Y. Q. Ma, K. Wang and K. T. Chao, Phys. Rev. D **83**, 111503 (2011).
 - [5] Z. G. He, Y. Fan and K. T. Chao, Phys. Rev. D **75**, 074011 (2007); Y. Q. Ma, K. Wang and K. T. Chao, Phys. Rev. Lett. **106**, 042002 (2011); Y. Q. Ma, K. Wang and K. T. Chao, Phys. Rev. D **84**, 114001 (2011).
 - [6] B. Gong, and J. X. Wang, Phys. Rev. Lett. **100**, 232001 (2008); B. Gong, and J. X. Wang, Phys. Rev. D **78**, 074011 (2008); B. Gong, X. Q. Li and J. X. Wang, Phys. Lett. B **673**, 197 (2009).
 - [7] R. Li, and J. X. Wang, Phys. Lett. B **672**, 51 (2009); B. Gong, and J. X. Wang, Phys. Rev. D **83**, 114021 (2011); B. Gong, L. P. Wan, J. X. Wang and H. F. Zhang, Phys. Rev. Lett. **112**, 032001 (2014).
 - [8] **LHCb Collaboration**, R. Aaij *et al.*, Phys. Lett. B **707**, 52 (2012).
 - [9] CMS Physics Analysis Summary, CMS PAS BPH-11-021, 2013.
 - [10] R. Li, Y. J. Zhang and K. T. Chao, Phys. Rev. D **80**, 014020 (2009).
 - [11] C. F. Qiao, L. P. Sun and P. Sun, J. Phys. G **37**, 075019 (2010).
 - [12] A. V. Berezhnuy, A. K. Likhoded, A. V. Luchinsky and A. A. Novoselov, Phys. Rev. D **84**, 094023 (2011).
 - [13] Y. J. Li, G. Z. Xu, K. Y. Liu and Y. J. Zhang, J. High Energy Phys. 1307 (2013) 051.
 - [14] J. P. Lansberg and H. S. Shao, Phys. Rev. Lett. **111**, 122001 (2013).
 - [15] C. H. Com, A. Kulesza and W. J. Stirling, Phys. Rev. Lett. **107**, 082002 (2011).
 - [16] D. d'Enterria and A. M. Snigirev, arXiv:1301.5845.
 - [17] S. Baranov, A. Snigirev, and N. Zotov, Phys. Lett. B **705**, 116 (2011).
 - [18] Z. B. Kang, Y. Q. Ma, J. W. Qiu and G. Sterman, Phys. Rev. D **90**, 034006 (2014).
 - [19] B. W. Harris and J. F. Owens, Phys. Rev. D **65** 094032 (2002).
 - [20] Y. Q. Ma, J. W. Qiu, and H. Zhang, arXiv:1311.7078.
 - [21] V. N. Gribov and L. N. Lipatov, Sov. J. Nucl. Phys. **15**, 438 (1972).
 - [22] L. N. Lipatov, Sov. J. Nucl. Phys. **20**, 94 (1975).
 - [23] Y. L. Dokshitzer, Sov. Phys. JETP **46**, 641 (1977).
 - [24] G. Altarelli and G. Parisi, Nucl. Phys. B **126**, 298 (1977).
 - [25] J. Pumplin, D.R. Stump, J. Huston, H. L. Lai, P. M. Nadolsky, and W. K. Tung, JHEP **0207**, 012 (2002).
 - [26] T. Hahn, Comput. Phys. Commun. **140**, 418 (2001).
 - [27] CTEQ Collaboration, H.L. Lai *et al.*, Eur. Phys. J. C **12**, 375(2000).
 - [28] J. Pumplin et al J. High Energy Phys. **07** 012 (2002).
 - [29] G. T. Bodwin, H. S. Chung, D. Kang, J. Lee and C. Yu, Phys. Rev. D **77** 094017 (2008).
 - [30] H. Han, Y. Q. Ma, C. Meng, H. S. Shao, and K. T. Chao, Phys. Rev. Lett. **114**, 092005 (2015).
 - [31] B. Gong, L. P. Wan, J. X. Wang and H. F. Zhang, Phys. Rev. Lett. **110**, 042002 (2013).
 - [32] M. Butenschoen, and B. A. Kniehl, Nucl. Phys. Proc. Suppl. **222**, 151 (2011);
 - [33] Y. Q. Ma, K. Wang and K. T. Chao, Phys. Rev. Lett. **106**, 042002 (2011).
 - [34] Y. Q. Ma, J. W. Qiu, G. Sterman and H. Zhang, Phys. Rev. Lett. **113**, 142002 (2014).
 - [35] Z. G. He and B. A. Kniehl, Phys. Rev. Lett. **115**, 022002 (2015).